Magnetization reversal and magnetoresistance behavior of perpendicularly magnetized [Co/Pd]4/Au/[Co/Pd]2 nanowires

X. M. Liu, P. Ho, J. S. Chen, and A. O. Adeyeye

Citation: Journal of Applied Physics **112**, 073902 (2012); doi: 10.1063/1.4754858
View online: http://dx.doi.org/10.1063/1.4754858
View Table of Contents: http://scitation.aip.org/content/aip/journal/jap/112/7?ver=pdfcov
Published by the AIP Publishing

Magnetization reversal and magnetoresistance behavior of perpendicularly magnetized $[Co/Pd]_4/Au/[Co/Pd]_2$ nanowires

X. M. Liu,[1] P. Ho,[2] J. S. Chen,[2] and A. O. Adeyeye[1,a)]
[1]*Information Storage Materials Laboratory, Department of Electrical and Computer Engineering, National University of Singapore, Singapore 117576, Singapore*
[2]*Department of Materials Science and Engineering, National University of Singapore, Singapore 117576, Singapore*

(Received 4 July 2012; accepted 29 August 2012; published online 1 October 2012)

We present a systematic investigation of the magnetization reversal mechanism and magnetoresistance behavior of perpendicularly magnetized Co/Pd multilayer films and nanowires (NWs) as a function of Cu buffer layer thickness and temperature. The effect of interlayer coupling is studied by varying the Au spacer layer thickness in between two Co/Pd multilayer stacks in the $[Co/Pd]_4/Au/[Co/Pd]_2$ structure. We observed that compared with continuous (un-patterned) films deposited at the same time, the NWs display much stronger temperature dependent interlayer coupling due to magnetostatic interactions through the stray fields. At low temperature, the competition between the interlayer coupling and coercive field difference between the soft and hard Co/Pd multilayer stacks determines the overall magnetization reversal process and magnetoresistance behavior. © *2012 American Institute of Physics*. [http://dx.doi.org/10.1063/1.4754858]

I. INTRODUCTION

Pseudo-spin-valve (PSV) nanostructures, which consist of two ferromagnetic (FM) layers separated by a nonmagnetic spacer layer, have received considerable interest due to their potential in future spintronic applications such as magnetic random access memory (MRAM) cells[1] and high sensitivity magnetic sensors.[2] Compared with the PSVs with in-plane anisotropy, perpendicularly magnetized PSVs are predicted to benefit more from less cell geometry dependence, improved thermal stability, and lower critical current density for spin transfer switching, with significant advantages for high packing density.[3] Accordingly, there has been a recent shift of research interest towards understanding of the magnetization reversal mechanism of PSVs with perpendicular magnetic anisotropy (PMA), especially on the effects of interlayer coupling between two perpendicularly magnetized ferromagnetic layers.[4–7] The interlayer coupling can have four different origins:[8] direct ferromagnetic coupling through pinholes in the thin metallic spacer,[9] indirect exchange coupling through Ruderman-Kittel-Kasuya-Yosida (RKKY) interactions,[10] orange peel (Néel) coupling due to correlated interfacial roughness,[11] and finally magnetostatic coupling through the stray fields.[12,13] For the latter case, although the magnetostatic interactions are mostly negligible when the two FM layers are uniformly magnetized, they become notably prominent in magnetic layers with multidomain configurations[13,14] or in patterned magnetic nanostructures.[15,16] The non-uniform magnetization distribution in one FM layer induces local stray fields mainly arising from domain walls (DWs), which directly affect magnetic switching of the other FM layer and hence the performance of the PSV films. The stray fields show a fast decay with increase in distance from the DW border and film surface.[12,17,18] It has been reported that local stray fields from DWs are efficient to induce domain replication from a hard FM layer to a neighboring soft FM layer in ferromagnetically coupled Co/Pd[19] and Co/Pt[13] based PSV films.

So far, most research work has focused on the investigation of interlayer coupling of continuous PSV films.[20–22] There have been very few reports on the study of interlayer coupling in patterned PSV nanostructures with perpendicular anisotropy. Park *et al.*[16] observed an asymmetric current induced domain wall de-pinning in Co/Ni multilayer PSV nano-wires (NWs) resulting from the stray dipolar fields generated by the reference layer. Large stray fields have also been reported in patterned Co/Ni multilayer nano-pillars[15] and Co/Pt dots.[23] However, to our knowledge, there has been no report on temperature-dependent study of the interlayer coupling and its influences on the reversal mechanism and magnetoresistance (MR) behavior of perpendicularly magnetized PSV nanostructures.

In this work, we have conducted a systematic investigation on the effects of interlayer coupling on the magnetization reversal mechanism and MR behavior of $[Co/Pd]_4/Au(t_{Au})/[Co/Pd]_2$ PSV NWs as a function of temperature (T) by varying the spacer layer thickness t_{Au}. We compared NWs results with continuous Co/Pd PSV films deposited under identical conditions and observed a significant increase in the interlayer coupling field resulting in a marked difference in the MR behavior at low T. The paper is organized as follows: In Sec. II, we described our experiment details including the fabrication process. In Sec. III, we presented our results supported with the detailed discussions. Section IV is the conclusion.

II. EXPERIMENTAL DETAILS

Arrays of $Cu(t_{Cu})/Pd(5\,nm)/[Co(0.5\,nm)/Pd(3\,nm)]_4$ multilayer NWs of width $w = 340\,nm$, length $l = 4\,mm$, and

a)Author to whom correspondence should be addressed. Electronic mail: eleaao@nus.edu.sg.

edge-to-edge spacing $s = 80$ nm were fabricated on silicon substrates using deep ultraviolet lithography at 248 nm wavelength followed by lift-off process.[24] The multilayer films were deposited using DC magnetron sputtering in a 3 mTorr Ar pressure at room temperature. The base pressure of the chamber was better than 2×10^{-8} Torr. In order to enhance perpendicular anisotropy, a Cu buffer layer with thickness t_{Cu} varied in the range from 5 nm to 40 nm followed by a 5 nm Pd seed layer were deposited prior to the Co/Pd multilayer stack. Based on the coercive field dependence on the $[Co/Pd]_n$ multilayer repeat n, arrays of NWs with a PSV structure of Cu(15 nm)/Pd(5 nm)/$[Co(0.5\,nm)/Pd(3\,nm)]_4$/Au($t_{Au}$)/$[Co(0.5\,nm)/Pd(3\,nm)]_2$ were further fabricated. The upper $[Co/Pd]_2$ stack and the bottom $[Co/Pd]_4$ stack serve as soft and hard FM layers, respectively. The Au spacer layer thickness was varied from 1 nm to 8 nm, while the Cu buffer layer is fixed at 15 nm. For direct comparison, the corresponding continuous Co/Pd PSV films were also deposited at the same time with the PSV NWs.

In order to determine the optimum growth condition, the structural properties and roughness of the Co/Pd multilayer films were studied as a function of Cu buffer layer thickness using x-ray diffractometer (XRD) and x-ray reflectometry (XRR), atomic force microscope (AFM), respectively. The collective magnetic switching behaviors of the Co/Pd multilayer NWs and PSV NWs were characterized using a focused polar magneto-optic Kerr effect (MOKE) set up with a spot size of about 5 μm and external magnetic field applied perpendicular to the plane of the samples. For the MR measurements, 200 nm thick Al electrical contacts were placed on top of the NWs using sputtering deposition. MR measurements were conducted using the standard four probe technique with a constant DC current of 1 mA (5 mA) for the NWs (corresponding continuous films), while the magnetic field is applied in the out-of-plane direction in the temperature range of $5\,K \le T \le 300\,K$.

III. RESULTS AND DISCUSSION

A. Effects of Cu buffer layer thickness on continuous films

In this section, we investigate the effects of Cu buffer layer thickness t_{Cu} on the magnetic properties of the Co/Pd multilayer films with a structure Cu(t_{Cu})/Pd(5 nm)/$[Co(0.5\,nm)/Pd(3\,nm)]_4$. A schematic of the multilayer structure with t_{Cu} varied in the range from 0 nm to 40 nm is shown in Fig. 1(a). Representative polar M-H hysteresis loops for the Co/Pd multilayer films as a function of t_{Cu} are shown in Fig. 1(b). Clearly, the coercive field of the films is strongly dependent on the Cu buffer layer thickness, showing a marked increase from 445 Oe to 869 Oe as the buffer layer thickness is increased from 0 nm to 15 nm, respectively. Further increase in Cu layer thickness does not result in significant enhancement of coercive field of the Co/Pd multilayer films. We observed that $t_{cu} = 15$ nm is the optimum buffer layer thickness. We have also measured the XRD patterns of the multilayer films as a function of t_{Cu}, as shown in Fig. 1(c). A clear CoPd(111) peak at around 2θ=40.6° is observed for all the Co/Pd multilayer films, which is a good indication of the growth of fcc(111) CoPd. No notable change in either the CoPd(111)

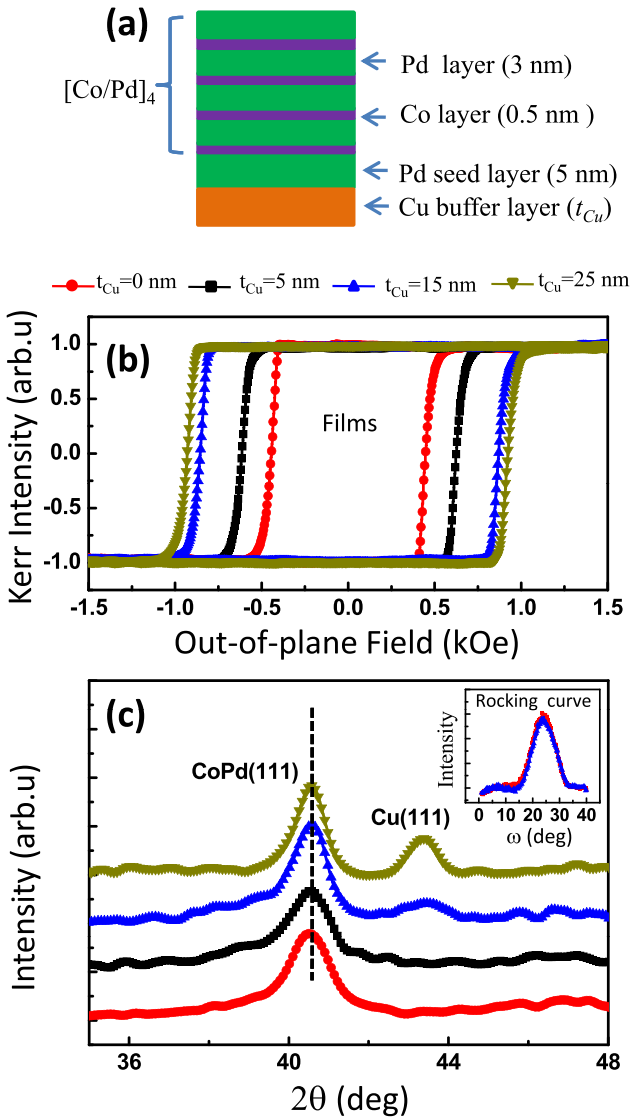

FIG. 1. (a) Schematics of deposited Cu(t_{Cu})/Pd(5 nm)/$[Co(0.5\,nm)/Pd(3\,nm)]_4$ multilayer structure; (b) polar M-H loops of the multilayer films as a function of Cu buffer layer thickness t_{Cu}; and (c) XRD patterns of the Co/Pd multilayer films as a function of t_{Cu} (the rocking curve XRD results for the Co/Pd multilayers with and without 15 nm Cu buffer layer are shown as an inset).

peak position or the intensity is observed as t_{Cu} is increased. Furthermore, we did not see any clear difference in the rocking curve XRD measurements for the Co/Pd multilayers by comparing films with and without 15 nm thick Cu buffer layer (see the inset of Fig. 1(c)). These results suggest that there is no texture change in the Co/Pd multilayer films due to the Cu buffer layer. For films with $t_{Cu} \ge 15$ nm, we noticed an additional peak between $2\theta = 43.4°$ and $2\theta = 43.5°$, corresponding to a fcc(111) peak of the Cu buffer layer.

We also studied the surface roughness of the Co/Pd multilayer films using AFM. Shown as insets in Fig. 2(a) are the representative AFM micrographs for the Co/Pd multilayer films with $t_{Cu} = 0$ nm and $t_{Cu} = 15$ nm taken over an area of 300 nm × 300 nm. It is obvious that the mean grain size of the Co/Pd multilayers is very sensitive to the Cu buffer layer thickness, similar to the previous observation in Cu buffered $SmCo_5$-film.[25] We have plotted the mean grain size and surface roughness extracted from the AFM micrographs of the

continuous Co/Pd films as a function of Cu buffer layer thickness t_{Cu} in Fig. 2(a). Both the mean grain size and root mean square (RMS) roughness show a rapid increase up to $t_{Cu} = 15$ nm, after which they tend to be stabilized.

This roughness dependence on t_{Cu} has been further confirmed using XRR measurements. Fig. 2(b) shows the representative XRR spectra for the Co/Pd multilayer films with $t_{Cu} = 0$ nm and $t_{Cu} = 15$ nm, respectively. Because of the large coherence length of the x-ray beam ($\sim 50\,\mu$m), the reflectivity curves are an effective probe to determine the layer thickness and interfacial roughness. The simulation fits were performed using a software package LEPTOS 4.02 (available from Bruker-AXS, Karlsruhe, Germany), where the thickness and interface roughness of each layer were allowed to vary. There is a comparatively good match between simulation and experimental results. The thickness of Co/Pd bi-layer was found to be approximately 6% smaller relative to the thickness determined from deposition rates calibrated using a surface profiler, which may be due to the use of bulk scattering and index of refraction constant in the fits. The plotted interface roughness vs t_{Cu} extracted from the XRR simulations is shown in the inset of Fig. 2(b). We observed a rapid increase of interface roughness from 0.8 nm to 1.4 nm as t_{Cu} is increased up to 15 nm, which follows similar trend with the RMS roughness measurements taken from AFM (see Fig. 2(a)). Again, the roughness value becomes almost stabilized for $t_{Cu} \geq 15$ nm. Interestingly, the interface roughness is larger than the RMS roughness, which has also been observed in Pd and Ta buffered Co/Pd multilayers.[26]

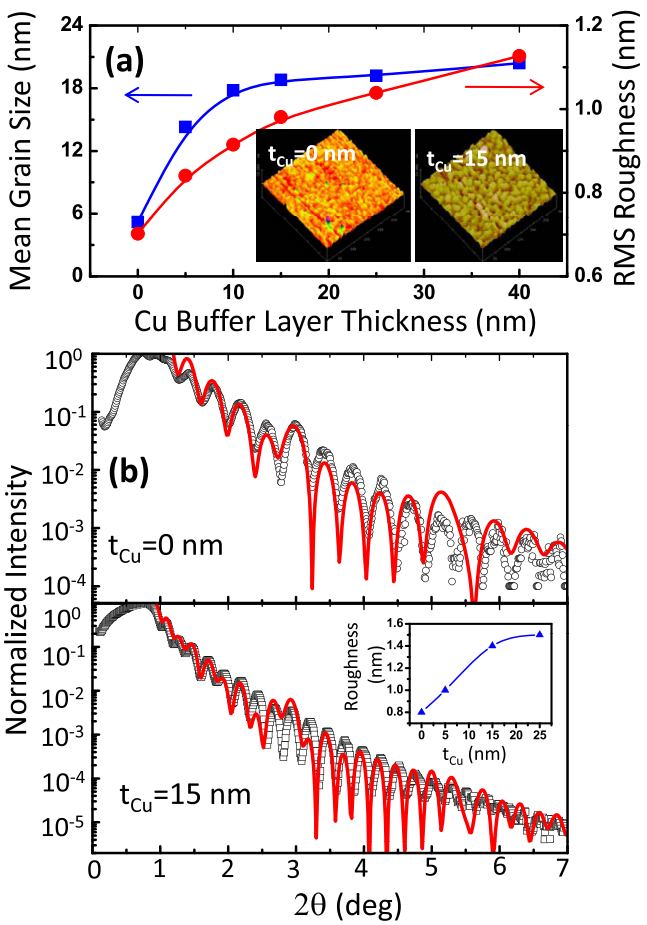

FIG. 2. (a) A plot of the mean grain size and RMS roughness of the Cu(t_{Cu})/Pd(5 nm)/[Co(0.5 nm)/Pd(3 nm)]$_4$ multilayer films as a function of t_{Cu} (two representative atomic force micrographs with $t_{Cu} = 0$ nm and $t_{Cu} = 15$ nm are shown as insets). (b) Representative XRR spectra and best fits for the multilayer films with $t_{Cu} = 0$ nm and $t_{Cu} = 15$ nm (the extracted interface roughness as a function of t_{Cu} is shown as an inset).

We believe that the combined effect of increased mean grain size and film roughness is responsible for the changes in magnetic properties of the Co/Pd multilayer films.[27,28] The magnetic properties of an assembly of small grains depend strongly on the counterplay of local magnetic anisotropy energy and ferromagnetic exchange energy. The effective anisotropy for the magnetic behaviors is an average over several grains. Larger grain size favors increased coercive field due to enhanced effective anisotropy resulting from reduced lateral exchange interactions between grains.[29] On the other hand, film roughness may constrain domain wall motion hence retard the magnetic switching of the multilayer films. This claim is based on the fact that magnetization reversal of Co/Pd multilayer films occurs via reversed domain nucleation followed by rapid domain wall motion.[30]

B. Effects of Cu buffer layer thickness on patterned NWs

Now, we focus on the magnetization reversal process of [Co/Pd]$_n$ multilayer NWs with $n = 4$ as a function of Cu buffer layer thickness. Shown in Fig. 3(a) are the polar MOKE hysteresis loops for arrays of [Co/Pd]$_4$ NWs as a function of t_{Cu}. A representative scanning electron micrograph (SEM) of the NWs ($t_{Cu} = 15$ nm) is shown as an inset. Again, we observed an increase in coercive field H_c for the NWs due to the effects of the Cu buffer layer thickness. We have extracted the H_c from the hysteresis loops and plotted it as a function of t_{Cu} for both the NWs and the continuous films in Fig. 3(b). A rapid increase of H_c with t_{Cu} is observed when $t_{Cu} \leq 15$ nm. Further increase in t_{Cu} does not significantly affect the coercive fields of both the NWs and the films. Interestingly, this coercive field dependence on Cu buffer layer thickness is in agreement with the earlier results on mean grain size and film roughness (see Fig. 2), suggesting that mean grain size and film roughness play an important role in determining the magnetization reversal of Co/Pd multilayer films and NWs.

We have also compared the M-H loops of the [Co/Pd]$_2$ NWs and continuous films with $t_{Cu} = 15$ nm as shown in the inset of Fig. 3(b). Interestingly, in contrast with the [Co/Pd]$_4$ NWs where the coercive field is much larger than the corresponding continuous film, the H_c of [Co/Pd]$_2$ NWs is smaller than the continuous film. This could be due to a reduction in the perpendicular anisotropy or canted anisotropy axis at the edge of the NWs. It has been reported that variation in PMA or anisotropy axis of defects can cause a significant change in reversal field of patterned Co/Pd multilayer nanostructures.[31]

C. Effects of Au spacer layer thickness on interlayer coupling

We have shown in Sec. III B that the coercive field of [Co/Pd]$_n$ multilayer is dependent on number of bi-layer repeat n.

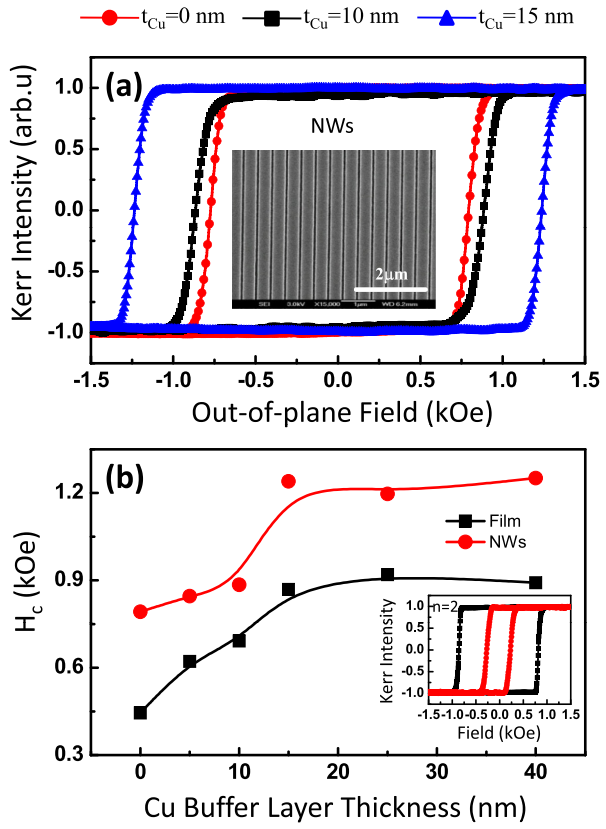

FIG. 3. (a) Polar M-H loops of arrays of Cu(t_{Cu})/Pd(5 nm)/[Co(0.5 nm)/Pd(3 nm)]$_4$ NWs as a function of t_{Cu} (a scanning electron micrograph of the NWs is shown as an inset).(b) Coercive field H_c vs t_{Cu} for both the [Co/Pd]$_4$ multilayer NWs and corresponding continuous films (M-H loops of the [Co/Pd]$_2$ multilayer NWs and films with $t_{Cu} = 15$ nm are shown as an inset).

Using this information, we have designed Co/Pd PSV structures consisting of Cu(15 nm)/Pd(5 nm)/[Co(0.5 nm)/Pd(3 nm)]$_4$/Au(t_{Au})/[Co(0.5 nm)/Pd(3 nm)]$_2$, as shown as a schematic in Fig. 4(a). The upper Co/Pd multilayer stack ($n = 2$) and bottom Co/Pd multilayer stack ($n = 4$) serve as soft and hard FM layers, respectively. The Au spacer layer thickness t_{Au} was varied in the range from 1 nm to 8 nm. Shown in Figs. 4(b) and 4(c) are the representative polar MOKE hysteresis loops and MR responses taken at room temperature for the Co/Pd PSV NWs with $t_{Au} = 1.5$ nm. For direct comparison, the hysteresis loops and MR responses of the corresponding continuous film are also shown (see Figs. 4(d) and 4(e)). The MR ratio is defined as

$$MR = \frac{R(H) - R(H_{\max})}{R(H_{\max})} \times 100\%, \qquad (1)$$

where $R(H)$ and $R(H_{max})$ are the resistance of the sample at an applied out-of-plane field of H and the maximum field H_{max}, respectively. For both the PSV NWs and the continuous film, we observed a distinct two-step switching, corresponding to the magnetization reversal of the soft Co/Pd multilayer stack ($n = 2$) at low field and the hard Co/Pd multilayer stack ($n = 4$) at high field, respectively. Schematics of the magnetization states are shown as insets in Fig. 4(b). Interestingly, the Kerr intensity drop of the soft Co/Pd multilayer stack ($n = 2$) at the top is larger than that of the hard multilayer stack ($n = 4$) at the bottom of the continuous PSV film because the MOKE setup is more sensitive to surface material. To confirm that the soft Co/Pd multilayer stack ($n = 2$) indeed switches first, the M-H loop measurement of the continuous film was repeated using a vibrating sample magnetometer (VSM) as shown in the inset of Fig. 4(d). As expected, the first switching step at low field occurs with smaller moment drop, implying that the soft Co/Pd multilayer stack ($n = 2$) switches first. There is also a good agreement between the hysteresis loops and the MR responses (Figs. 4(b)–4(e)). The MR plateau arises from the antiparallel relative alignment of magnetization of the two Co/Pd multilayer stacks. At saturation field, the two Co/Pd multilayer stacks are aligned parallel to the field direction resulting in the low MR ratio. Interestingly, the PSV NWs show a much larger MR ratio (0.29%) compared to the corresponding continuous film (0.13%), which may be due to the enhanced spin scattering at the edge of the NWs. In the patterned nanostructures, electrons are physically confined by the edge boundaries, which may increase the possibility of spin reflection at the interfaces, leading to a higher MR ratio. Similar spin reflection induced MR enhancement has also been observed in nanostructures with current-confined-path nano-oxide layers.[32,33]

Due to the different switching fields, the interlayer coupling (sign and strength) between the two Co/Pd multilayer stacks can be determined by conducting detailed minor M-H loop measurements. To measure the minor loop, a large negative field is first applied to saturate both the soft and hard Co/Pd multilayer stacks, followed by application of a suitable positive field to switch only the upper soft Co/Pd stack, after which, the field is reversed until negative saturation to switch the soft stack again. If there is coupling between the soft and hard Co/Pd multilayer stacks, the minor M-H loop center will be shifted away from the zero-field axis, which is a measure of the inter-layer coupling field (H_{coup}). When the $H_{coup} > 0$, there is a ferromagnetic coupling between the two layers. However, for $H_{coup} < 0$, this is an indication that the coupling is antiferromagnetic. From the minor M-H loop shown in Fig. 4(b), a positive interlayer coupling field as large as 290 Oe is observed for the PSV NWs, indicating that there is a strong FM coupling between the soft Co/Pd multilayer stack ($n = 2$) and the hard Co/Pd multilayer stack ($n = 4$). Again, there is a good agreement between the minor M-H loops of the MOKE signal and the MR response. Interestingly, the continuous film deposited at the same time as the PSV NWs shows a much weaker coupling field of 14 Oe originating from interlayer coupling due to possible pin holes, RKKY coupling, or Néel type coupling. Since the NWs were fabricated under the same conditions as the continuous film, these three interlayer coupling mechanisms should have similar coupling strength in the PSV NWs. The only difference between the Co/Pd NWs and the continuous film is the interlayer magnetostatic interactions through stray fields in the NWs, which is negligible in the continuous Co/Pd PSV film.

We have systematically probed the influence of Au spacer layer thickness t_{Au} on the interlayer magnetostatic coupling and magnetization reversal of the Co/Pd PSV NWs.

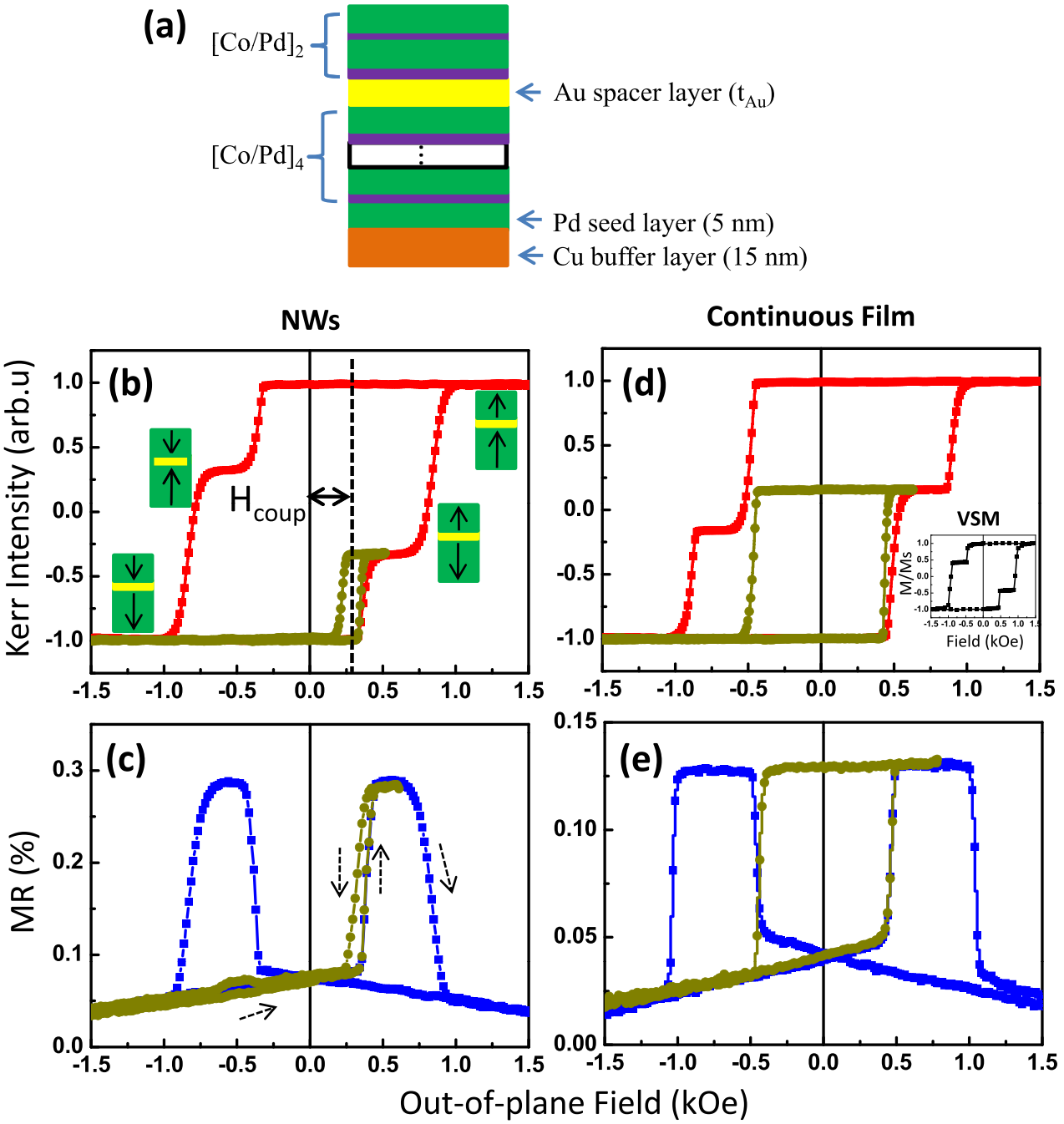

FIG. 4. (a) Schematics of deposited Cu/Pd/[Co/Pd]$_4$/Au(t_{Au})/[Co/Pd]$_2$ PSV structure; (b) polar M-H loops of the PSV NWs with $t_{Au} = 1.5$ nm (minor loop shift represents the interlayer coupling field H_{coup}); (c) MR responses of the PSV NWs with $t_{Au} = 1.5$ nm. The hysteresis loops and MR responses of the corresponding continuous film with $t_{Au} = 1.5$ nm are shown in (d) and (e), respectively (VSM result for the PSV film is shown as an inset in (d)).

Shown in Figs. 5(a)–5(e) are the major and minor M-H loops of the PSV NWs with t_{Au} varied in the range from 1 nm to 3.5 nm. For $t_{Au} = 1$ nm, we observed only a single-step switching for the PSV NWs, compared to the two steps seen in the corresponding continuous film as shown in the inset of Fig. 5(a). This is a direct effect of the strong interlayer magnetostatic coupling and possible ferromagnetic coupling, which induces collective magnetization reversal of the soft and hard Co/Pd multilayer stacks. For the uniformly magnetized PSV film with $t_{Au} = 1$ nm, however, the magnetostatic coupling via stray fields is very negligible. A much weaker positive inter-layer coupling field of 20 Oe was measured. This interlayer coupling is considerably weak to overcome the coercive field difference between the two Co/Pd multilayer stacks, thereby resulting in a clear two-step switching. For the PSV NWs with $1.5\,\text{nm} \leq t_{Au} \leq 3.5\,\text{nm}$, due to a reduction in the stray fields, two distinct switching steps are seen corresponding to the magnetic switching of the soft Co/Pd stack at lower field and the hard Co/Pd stack at higher field, respectively. As t_{Au} is increased, the minor loop center shifts towards zero field, which verifies the weakened magnetostatic coupling between the two Co/Pd multilayer stacks.

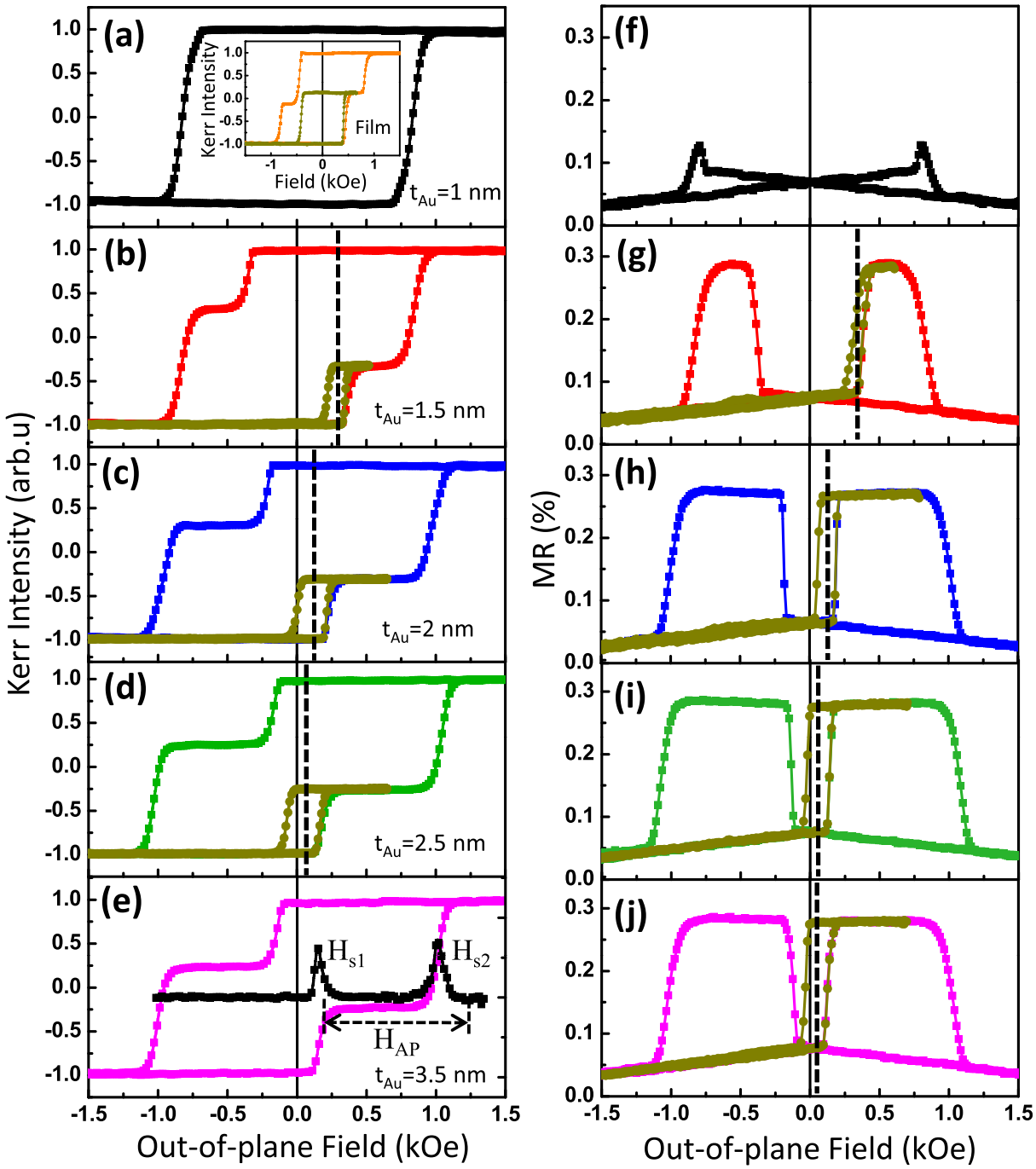

FIG. 5. Polar M-H loops of the Cu/Pd/[Co/Pd]$_4$/Au(t_{Au})/[Co/Pd]$_2$ PSV NWs with (a) $t_{Au} = 1$ nm (M-H loops of the corresponding continuous film are shown as an inset); (b) $t_{Au} = 1.5$ nm; (c) $t_{Au} = 2$ nm; (d) $t_{Au} = 2.5$ nm; and (e) $t_{Au} = 3.5$ nm. The corresponding MR loops are shown in (f)-(j), respectively. The dashed lines indicate the reduced interlayer coupling with t_{Au}.

The corresponding MR responses for the PSV NWs with $1\,\text{nm} \leq t_{Au} \leq 3.5\,\text{nm}$ are shown in Figs. 5(f)–5(j). In agreement with the M-H loop in Fig. 5(a), the MR curve for $t_{Au} = 1$ nm displays a sharp peak with a small MR ratio of 0.13% due to the strong interlayer coupling between the soft and hard Co/Pd stacks. For the PSV NWs with $1.5\,\text{nm} \leq t_{Au} \leq 3.5\,\text{nm}$, the MR curves display typical giant magnetoresistance (GMR) behavior with distinct region of anti-parallel relative alignment of magnetization between the soft and hard Co/Pd stacks and a larger MR ratio (~0.29%). Again, we observed a reduced interlayer coupling field based on the minor loop center shift as the Au spacer layer thickness is increased, as indicated by the dashed lines in Figs. 5(f)–5(j). Interestingly, the MR ratio almost keeps constant with t_{Au}.

In order to further understand the influence of Au spacer layer thickness t_{Au} on the interlayer magnetostatic coupling strength of the Co/Pd multilayer PSV NWs, we have performed numerical calculations on the stray fields from the bottom hard Co/Pd multilayer stacks ($n = 4$). We assume

that the hard Co/Pd FM stacks are uniformly magnetized with a constant magnetization M_0 perpendicular to the film plane. Our assumption is reasonable since the $[Co/Pd]_4$ multilayer stacks possess high perpendicular anisotropy. Shown in Fig. 6(a) is a schematic of the modeled $[Co/Pd]_4$ multilayer NWs with a cuboid structure of length, width, and thickness of $2L$, $2W$, and $2D$, respectively. The X and Y of Cartesian frame are along the length and width directions, while the Z axis (out-of-plane) corresponds to the thickness of NWs. For uniform magnetization, the $[Co/Pd]_4$ multilayer NWs is equivalent to two rectangular sheets at a distance $2D$ with homogenous magnetic charge densities $\pm M_0$ distributed at the upper and lower surfaces. The charge configuration induces an expression for the stray fields[34]

$$H(\vec{r}) = \frac{M_0}{4\pi} \cdot \int_{-L}^{+L} dx' \int_{-W}^{+W} dy' \times \left[\frac{\vec{r} - (x', y', c)}{|\vec{r} - (x', y', c)|^3} - \frac{\vec{r} - (x', y', -c)}{|\vec{r} - (x', y', -c)|^3} \right]. \quad (2)$$

By performing integral operation, the out-of-plane projection of the stray fields is given as follows:[34,35]

$$H_z(x,y,z) = -\frac{M_0}{4\pi} \cdot \sum_{m,n,k=1}^{2} (-1)^{m+n+k} \frac{[z-(-1)^k D] \cdot [x-(-1)^m L]}{|z-(-1)^k D]| \cdot |x-(-1)^m L|} \times \arctan\left\{ \frac{|x-(-1)^m L| \cdot [y-(-1)^n W]}{|z-(-1)^k D| \cdot \sqrt{[x-(-1)^m L]^2 + [y-(-1)^n W]^2 + [z-(-1)^k D]^2}} \right\}. \quad (3)$$

Since the $[Co/Pd]_4$ NWs are infinite long compared to the width and film thickness, the out-of-plane component of the stray fields can be simplified as follows:

$$H_z(x,y,z) = -\frac{M_0}{2\pi} \cdot \left[\arctan\frac{y-W}{t_{Au}} - \arctan\frac{y+W}{t_{Au}} - \arctan\frac{y-W}{t_{Au}+2D} + \arctan\frac{y+W}{t_{Au}+2D} \right], \quad (4)$$

where M_0 is the saturation magnetization of the $[Co/Pd]_4$ multilayer film which was extracted experimentally from the VSM measurement. Shown in the inset of Fig. 6(b) is the calculated Z-axis component of the stray field generated by the hard Co/Pd FM stacks ($n = 4$) in the soft Co/Pd stacks ($n = 2$) with a spacer layer thickness $t_{Au} = 1.5$ nm across the NW width. In our approximation, the magnetostatic interactions from the hard Co/Pd FM stacks of the nearest and second nearest neighboring PSV NWs was also taken into consideration in the calculation. The out-of-plane component of the stray fields (H_z) varies across the NW width in such a way that it is the weakest at the center and strongest at the edges in agreement with the observation in Co/Ni multilayer constrictions.[16] We have calculated H_z at the edge of the NWs (y = 169 nm) as a function of t_{Au}, as shown in Fig. 6(b) (empty circle). H_z shows a fast decay from 238 Oe down to 57 Oe as the Au spacer layer thickness is slightly increased from 1.5 nm to 3.5 nm.

The strong dependence of the stray fields on t_{Au} is further verified experimentally. We have extracted the interlayer coupling field (H_{coup}) as a function of t_{Au} from the minor M-H loops in Fig. 5 and plotted it in Fig. 6(b) (solid circle). We found a significant decrease of H_{coup} from 290 Oe for $t_{Au} = 1.5$ nm to 48 Oe for $t_{Au} = 2.5$ nm, after which only a slight decrease of H_{coup} is seen, implying that the two FM stacks are magnetically de-coupled. This is further confirmed by the PSV NWs with $t_{Au} = 8$ nm (not shown), where only a small H_{coup} of 11 Oe is observed. There is only qualitative agreement between the experimental and calculation results. This is expected since the calculation only considers the stray field at one point (y = 169 nm) while the interlayer

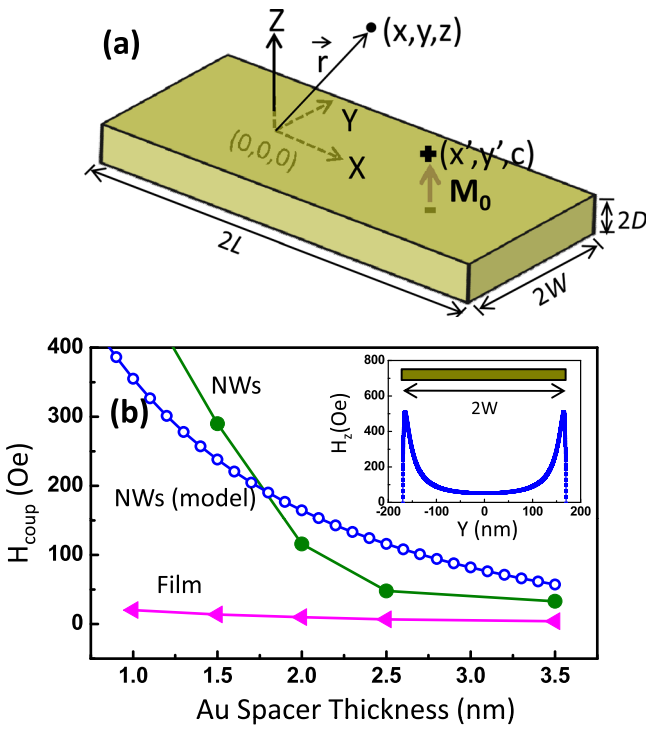

FIG. 6. (a) Schematics for stray field calculation of the $[Co/Pd]_4$ NWs. (b) A plot of calculated stray fields (empty circle), interlayer coupling field H_{coup} extracted experimentally from minor M-H loop shift of the Cu/Pd/$[Co/Pd]_4$/Au(t_{Au})/$[Co/Pd]_2$ NWs (solid circle) and corresponding continuous films (solid triangle) as a function of Au spacer layer thickness t_{Au}.

magnetostatic coupling of the PSV NWs is the average effect of stray fields across the NW width, and the modeling does not take into account the defect distribution in the actual sample. For comparison, the H_{coup} of the corresponding continuous films is also shown in Fig. 6(b) (solid triangle). The PSV films show a much smaller H_{coup} due to the absence of interlayer magnetostatic coupling via the stray fields, with a monotonous decrease from 20 Oe to 4 Oe as t_{Au} is increased from 1 nm to 3.5 nm.

Interlayer magnetostatic coupling also plays an important role in engineering the magnetic switching of both the soft and the hard Co/Pd multilayer stacks of the PSV NWs. To determine the switching process, the differential (dM/dH) of the M-H loop as a function of the applied field from the negative to positive saturation field is also plotted in Fig. 5(e). The two peaks observed correspond to the different switching processes occurring as the field is swept. We defined three parameters H_{s1}, H_{s2}, and H_{AP}, corresponding to the switching fields of the soft Co/Pd stack ($n=2$), the hard Co/Pd stack ($n=4$), and the stable field range over which the two Co/Pd multilayer stacks are in anti-parallel relative alignment of magnetization, respectively. Shown in Fig. 7 is a plot of the extracted H_{s1}, H_{s2}, and H_{AP} as a function of t_{Au}. For $t_{Au} \leq 2.5$ nm, a marked decrease of H_{s1} and a notable increase of H_{s2} with the Au spacer layer thickness are observed due to reduced interlayer coupling strength. Consequently, the stable field range (H_{AP}) shows a rapid increase from 0 for $t_{Au}=1$ nm to 610 Oe for $t_{Au}=2.5$ nm and becomes stabilized afterwards.

D. Effects of temperature on interlayer coupling and MR behavior

We have conducted a detailed investigation on the effects of temperature (T) on interlayer coupling and MR behavior of the Co/Pd PSV NWs and continuous films. Shown in Fig. 8(a) are major and minor MR loops of the PSV NWs with $t_{Au}=1.5$ nm as a function of T. At high temperature, the MR response is dominated by the GMR effect. However, as temperature is decreased, a noticeable transition in the MR response to that dominated by magnon magnetoresistance (MMR)[36] and possible anisotropic magnetoresistance (AMR), intrinsic domain wall resistance (DWR) is observed at $T=5$ K. The major loop of the MR response taken at $T=200$ K shows a typical GMR behavior with a clear plateau field range of 254 Oe, indicating a separate magnetic switching of the soft and the hard Co/Pd multilayer stacks. Interestingly, we observed a linear non-saturating MR response after saturation due to MMR effect arising from spin wave damping at high fields corresponding to a decrease in the intrinsic spin disorder,[36] as shown as an enlarged half loop MR curve in the inset of Fig. 8(a). However, the MMR contribution is almost one order of magnitude smaller than the GMR response. As temperature is decreased to $T=150$ K, the MR plateau becomes rounded due to the combined effect of reduced coercive field difference and enhanced interlayer coupling.

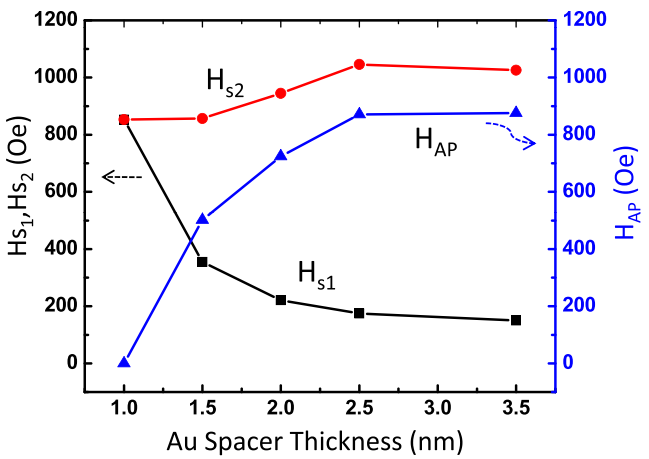

FIG. 7. A plot of Hs_1, Hs_2, and H_{AP} defined in Fig. 5(e) as a function of t_{Au}.

In Co/Pd multilayer films, due to a Co 3 *d*-Pd 4 *d* hybridization at the Co/Pd interfaces, the Pd layers are polarized, thus becoming weakly FM and favoring the FM interlayer coupling between the Co layers through the Pd layers. The Pd polarization can go into the Pd layer up to 0.7 nm at room temperature.[37] It has been previously reported[20,38] that for Co/Pt multilayer, the Pt polarization goes deeply into the Pt layers with decrease in temperature, consequently strengthening the FM interlayer coupling and reinforcing the coercive field of the Co/Pt multilayer stacks. This should also be valid for Co/Pd multilayers since both Pd and Pt have similar electronic configurations. The coercive field of both the soft Co/Pd multilayer stack ($n=2$) and the hard Co/Pd multilayer stack ($n=4$) increases with decrease in temperature. However, the soft Co/Pd stack shows a faster increase rate, leading to a reduction in the coercive field difference at lower temperature. The temperature dependence of coercive field on n has been previously reported in Co/Ni[39] and Co/Pt[40,41] multilayers.

We have also conducted minor loop measurements and extracted the inter-layer coupling field H_{coup} between the two Co/Pd FM stacks from minor loop center shift of the MR responses. Compared with $T=200$ K, minor loop of the PSV NWs shows an upwards shift of H_{coup} to 1.65 kOe at $T=150$ K, indicating an enhanced interlayer coupling. As temperature is further decreased, there is a drastic reduction in the MR ratio from 1.1% to 0.27% for $T=150$ K and $T=5$ K, respectively. The MR response taken at $T=5$ K resembles that of a single Co/Pd multilayer stack with an MR peak mainly arising from MMR and possibly AMR, DWR, which will be discussed later. This suggests a collective magnetization reversal of the soft and hard Co/Pd multilayer stacks due to a strong interlayer coupling between the two Co/Pd multilayer stacks, which is further verified by the gradual switching of the PSV NWs in the downward branch of the minor loop. Again, we observed the linear non-saturating MMR response from the inset, which becomes more prominent due to the absence of GMR effect.

For comparison, the major and minor MR loops of the corresponding continuous Co/Pd PSV film with $t_{Au}=1.5$ nm are also shown in Fig. 8(b). We observed typical GMR responses at all temperatures. Again, the plateau field range over which the two Co/Pd multilayer stacks are in antiparallel magnetization state decreases with temperature and becomes rounded at $T=5$ K, which further confirms the

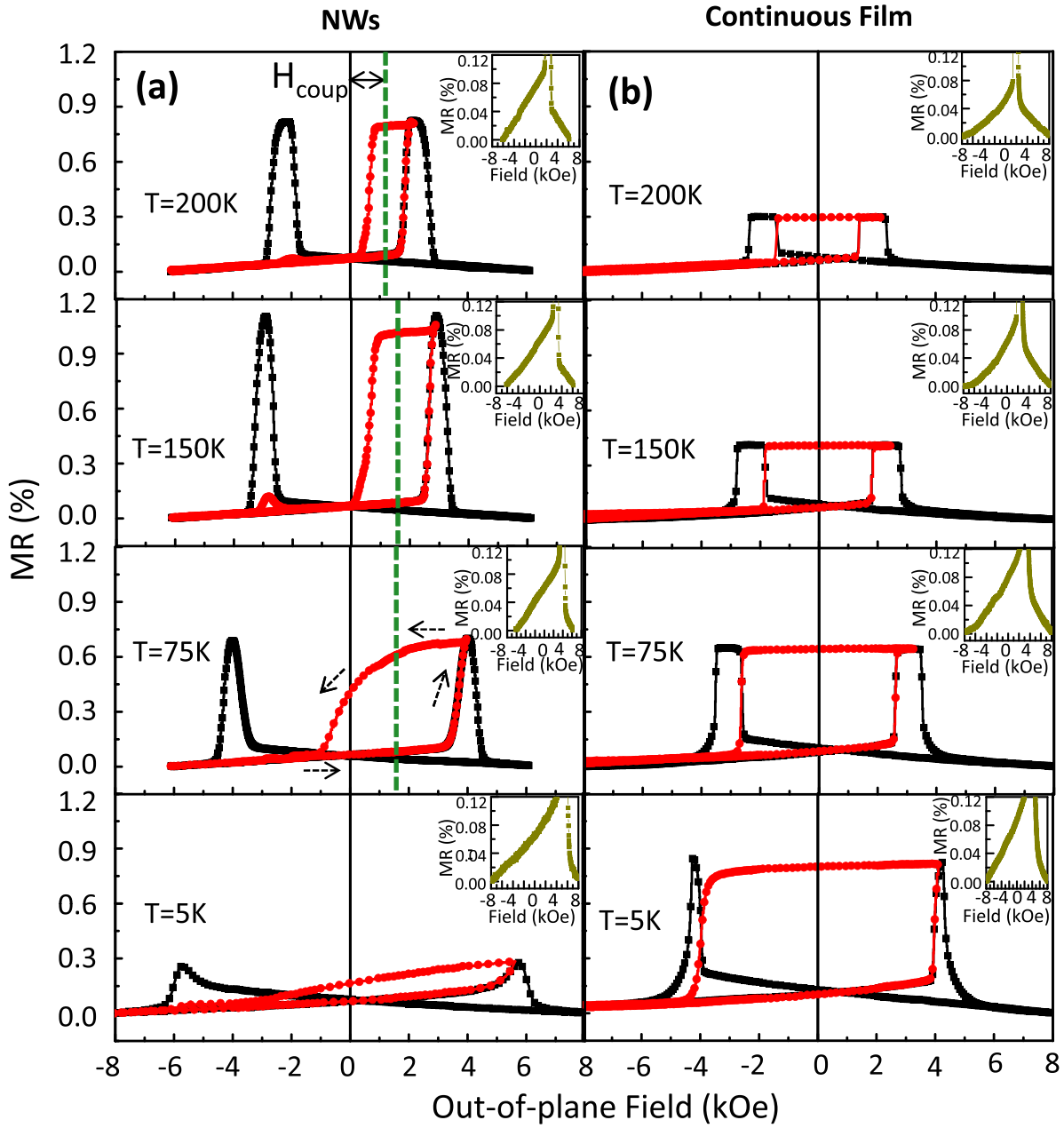

FIG. 8. Major and minor MR loops as a function of temperature T for the Cu/Pd/$[Co/Pd]_4$/Au(t_{Au})/$[Co/Pd]_2$ multilayers with $t_{Au} = 1.5$ nm for (a) NWs (the dashed line indicates interlayer coupling field H_{coup}) and (b) corresponding continuous film. The enlarged half-loop MR curves are shown as insets.

reduced coercive field difference between the soft and hard Co/Pd multilayer stacks at lower temperature. Interestingly, the MR ratio of the continuous film increases from 0.3% to 0.82% as the temperature is decreased from $T = 200$ K to $T = 5$ K. This is in direct opposite of the observation in the PSV NWs as shown in Fig. 8(a). The linear non-saturating MMR behavior is also observed at all temperatures, as shown in the insets of Fig. 8(b).

In order to further understand the MR behaviors of the PSV NWs at low temperature, we have performed MR measurements on the Co/Pd multilayer stack ($n = 4$) corresponding to the hard FM layer of the PSV stack. Shown in Figs. 9(a) and 9(b) are MR responses of the $[Co/Pd]_4$ multilayer NWs and corresponding continuous film as a function of temperature, respectively. At $T = 200$ K, we observed a sharp switching followed by a linear non-saturating MR response above magnetic saturation due to MMR effect. The resistivity variation of perpendicularly magnetized Co/Pd NWs with magnetic field is mainly resulted from three contributions, namely, AMR, DWR, and MMR.[36] Since the magnetization of the Co/Pd NWs is perpendicular to the applied sense current, the MR contribution from AMR is negligible. The MR contribution from DWR can also be excluded at high fields since no domain wall exists at saturation states. Therefore, the linear non-saturating MR response mainly arises from the MMR effect. As the temperature is decreased ($T = 100$ K), the MMR effect is less obvious, as seen from the decreased linear MMR slope and the appearance of a transformation peak due to reduced magnon-drag effect.[42] At $T = 5$ K, the MR curve resembles that obtained from the PSV NWs in Fig. 8(a), suggesting that the PSV NWs perform like a single FM stack at $T = 5$ K due to strong interlayer coupling. Shown as

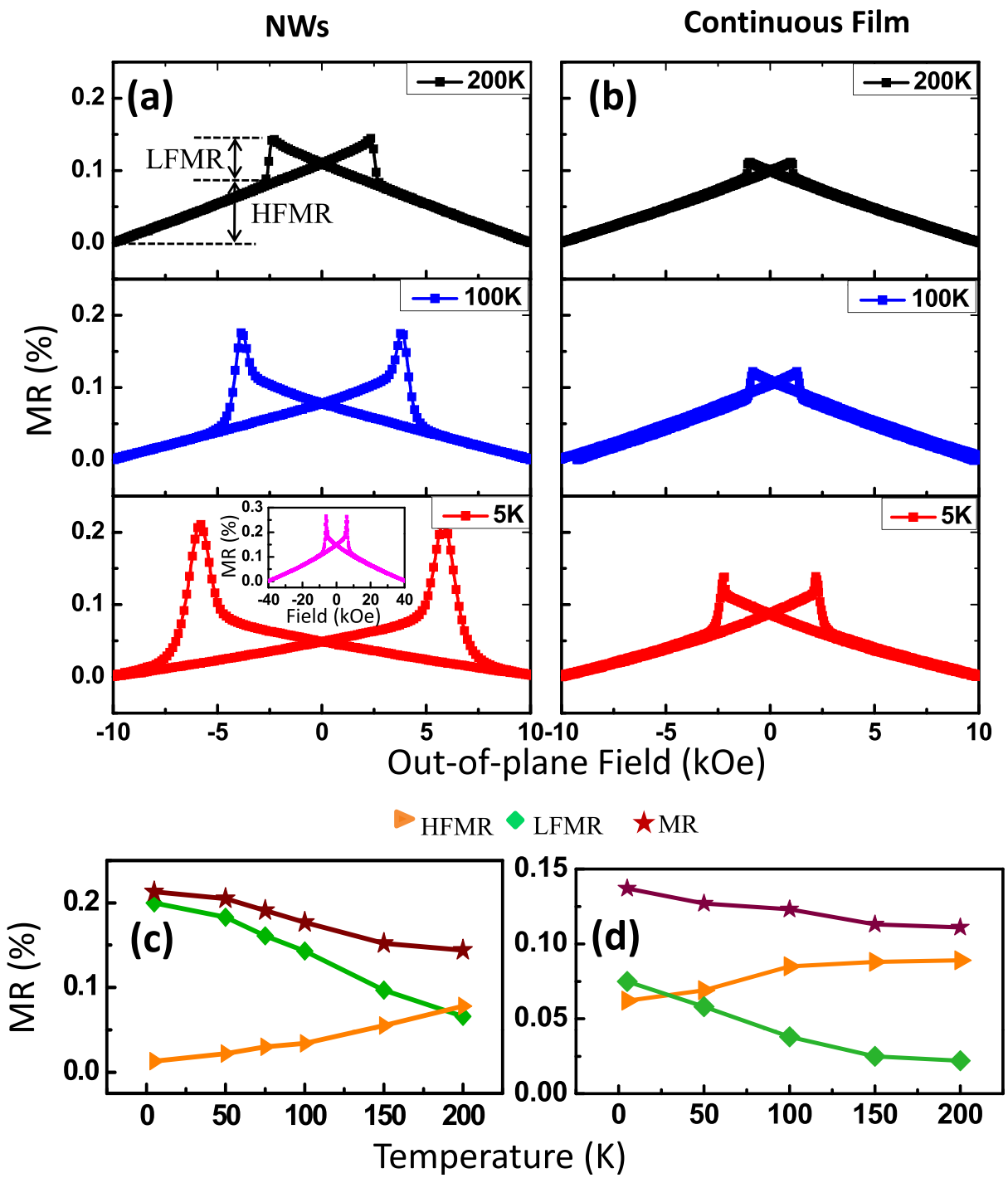

FIG. 9. MR loops as a function of temperature for (a) $[Co/Pd]_4$ multilayer NWs (the MR loop taken at $T = 5$ K in the field range of ± 40 kOe is shown as an inset) and (b) the continuous film. A plot of the MR, LFMR, and HFMR ratios (extracted from (a) and (b)) as a function of T for the NWs and continuous film are shown in (c) and (d), respectively.

inset in Fig. 9(a) is the MR loop taken in the field range of ± 40 kOe at $T = 5$ K. Again, we observed the linear non-saturating MMR response, which further confirms that the MMR effect dominants the MR response of the Co/Pd multilayer NWs. A large temperature dependent MMR effect is also observed in the $[Co/Pd]_4$ continuous film as shown in Fig. 9(b).

We have divided the MR response into two parts (as defined in Fig. 9(a)), namely, high field MR contribution (HFMR) and low field MR contribution (LFMR) for both the $[Co/Pd]_4$ NWs and corresponding continuous film, as shown in Figs. 9(c) and 9(d), respectively. The HFMR mainly arises from MMR, while the LFMR is a combined effect of MMR and possibly AMR and DWR effects. As temperature is decreased, HFMR effects are less pronounced and the MR responses of both the $[Co/Pd]_4$ NWs and continuous film are dominated by the contributions from LFMR leading to a increase of MR ratio.

We have extracted the interlayer coupling fields from the minor loop MR curves in Fig. 8. This has been plotted as a function of temperature for both the PSV NWs and corresponding continuous film, as shown in Fig. 10(a). For the continuous film, the interlayer coupling fields are small and almost independent on temperature, suggesting that the interlayer coupling originating from possible pin holes, RKKY coupling, or Néel type coupling is negligible at low T. For the PSV NWs, however, the interlayer coupling is significantly larger and markedly dependent on T. We observed a fast increase of interlayer coupling as T is decreased from 300 K to 100 K, which is followed by a slight change of H_{coup} at 25 K $\leq T \leq$ 100 K. Below $T = 25$ K, H_{coup} of the PSV NWs is difficult to distinguish due to the small squareness of the minor loop. Since the PSV NWs are deposited at the same time with the continuous film, the huge dependence of interlayer coupling on T may arise from the magnetostatic interactions through the stray fields. The reduced effective spacer layer thickness together with enhanced saturation magnetization of the hard Co/Pd multilayer stacks ($n = 4$) may be responsible for the large increase of H_{coup} at $T \geq 100$ K. In the PSV structure, the Au spacer layer is sandwiched by a 0.5 nm thick Co layer and a 3 nm thick Pd layer. Since only partial Pd layer is strongly polarized by the neighboring Co layer,[37] the effective spacer layer between the two FM stacks shall consist of both the Au layer and the weakly polarized part of the Pd layer. This assumption has been further verified by inserting a 0.5 nm thick Co layer to the upper interface of the bottom Co/Pd stack ($n = 4$), so that the Au spacer is sandwiched by two Co layers. We observed only a single step switching in such PSV NWs at room temperature (not shown here), suggesting a much stronger interlayer magnetostatic coupling in comparison with that without the Co insertion layer, where a distinct two-step switching is seen (see Fig. 4(b)). This is a direct effect of reduced effective spacer layer thickness. Although the Au layer thickness remains constant with temperature, the Pd polarization goes deeper into the Pd layer at low T, resulting in a reduced effective spacer layer thickness and hence enhanced interlayer magnetostatic coupling. On the other hand, the increased saturation magnetization with temperature[20] may also contribute to the increased interlayer coupling according to Eq. (4). The slight change of H_{coup} at 25 K $\leq T \leq$ 100 K may indicate the almost constant saturation magnetization[20] and effective spacer layer thickness at low T.

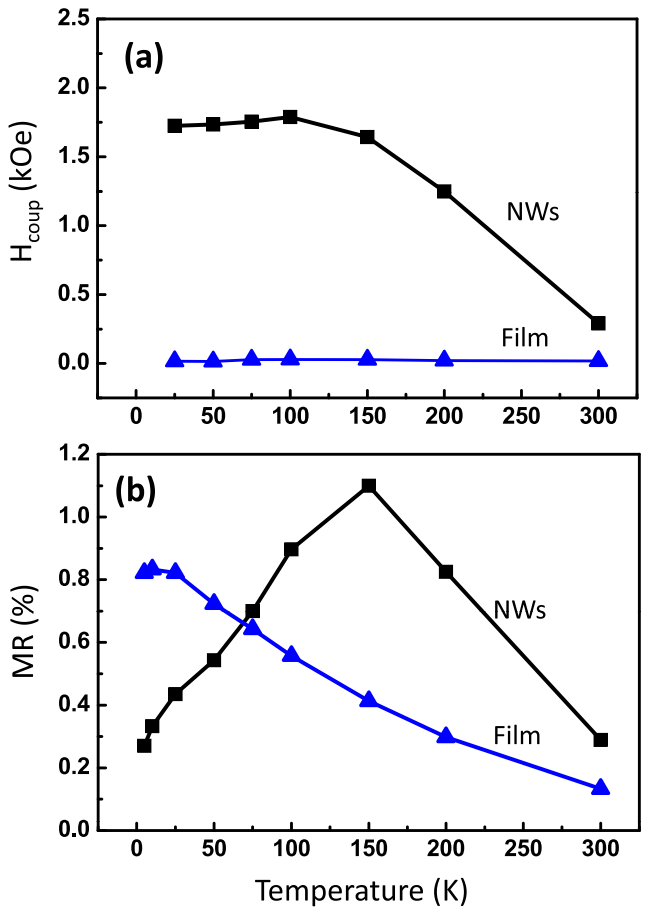

FIG. 10. A plot of (a) interlayer coupling field H_{coup} extracted from the minor loop shift of the MR responses and (b) MR ratio as a function of temperature for the Cu/Pd/$[Co/Pd]_4$/Au(t_{Au})/$[Co/Pd]_2$ PSV NWs and film with $t_{Au} = 1.5$ nm.

The effects of interlayer coupling on the MR ratio of the PSV NWs and continuous film as a function of temperature have also been analyzed, as shown in Fig. 10(b). Compared with the continuous PSV film, where typical GMR responses with a monotonous increase of MR ratio with T are observed, the PSV NWs show more complicated MR dependence on T due to the presence of interlayer magnetostatic coupling. We observed a MR ratio peak for the PSV NWs with $t_{Au} = 1.5$ nm (at $T = 150$ K) corresponding to the transition between GMR and MMR dominated effects. At high T, GMR effect dominates the MR response of the PSV NWs. However, at low T, MMR and possibly AMR, DWR effects may begin to play a more important role in affecting the MR response, resulting in a reduction of MR ratio. Interestingly, the PSV NWs show larger MR ratio at higher temperature ($T \geq 75$ K) compared to the corresponding continuous film due to the enhanced spin scattering at the edge of the NWs as discussed before.

IV. CONCLUSIONS

We have investigated the magnetization reversal process and magnetotransport properties of perpendicularly magnetized $[Co/Pd]_4$/Au/$[Co/Pd]_2$ films and nanowires (NWs) as a function of Cu buffer layer thickness and temperature. We show that coercive filed of the hard $[Co/Pd]_4$ stack of the PSV NWs can be greatly enhanced by adding Cu buffer layer due to combined effect of increased mean grain size and film roughness. The effect of interlayer coupling at various temperatures has been investigated by varying the Au spacer layer thickness in between the two Co/Pd FM stacks. We observed that for the continuous film deposited under the same condition, the interlayer coupling is almost independent of temperature. The interlayer coupling of PSV NWs however is much larger and strongly sensitive to temperature due to magnetostatic interactions through the stray fields. The competition between the interlayer coupling and coercive field difference of the soft and hard Co/Pd stacks determines the overall magnetization reversal process and magnetoresistance behavior of the PSV NWs.

ACKNOWLEDGMENTS

This work was supported by the National Research Foundation (NRF), Singapore under Grant No. NRFG-CRP 2007-05. The authors would like to thank Dr. N. Singh for his help with template fabrication. X. M. Liu is grateful for the research scholarship from the National University of Singapore.

[1]X. C. Zhu and J. G. Zhu, IEEE. Trans. Magn. **39**, 2854 (2003).
[2]M. M. Miller, G. A. Prinz, S. F. Cheng, and S. Bounnak, Appl. Phys. Lett. **81**, 2211 (2002).
[3]H. Meng and J. P. Wang, Appl. Phys. Lett. **88**, 172506 (2006).
[4]P. Ho, G. C. Han, G. M. Chow, and J. S. Chen, Appl. Phys. Lett. **98**, 252503 (2011).
[5]N. Thiyagarajah, S. Bae, H. W. Joo, Y. C. Han, and J. Kim, Appl. Phys. Lett. **92**, 062504 (2008).
[6]O. Hellwig, A. Berger, and E. E. Fullerton, Phys. Rev. Lett. **91**, 197203 (2003).
[7]Z. Y. Liu and S. Adenwalla, Phys. Rev. Lett. **91**, 037207 (2003).
[8]P. Y. Yang, X. Y. Zhu, F. Zeng, and F. Pan, Appl. Phys. Lett. **95**, 172512 (2009).
[9]P. W. T. Pong, C. L. Dennis, A. Castillo, A. Chen, and W. F. Egelhoff, J. Appl. Phys. **103**, 07A902 (2008).
[10]L. E. Nistor, B. Rodmacq, S. Auffret, A. Schuhl, M. Chshiev, and B. Dieny, Phys. Rev. B. **81**, 220407 (2010).
[11]J. Moritz, F. Garcia, J. C. Toussaint, B. Dieny, and J. P. Nozières, Europhys. Lett. **65**, 123 (2004).
[12]L. Thomas, M. G. Samant, and S. S. P. Parkin, Phys. Rev. Lett. **84**, 1816 (2000).
[13]V. Baltz, A. Marty, B. Rodmacq, and B. Dieny, Phys. Rev. B **75**, 014406 (2007).
[14]Y. Fu, W. Pei, J. Yuan, T. Wang, T. Hasegawa, T. Washiya, H. Saito, and S.Ishio, Appl. Phys. Lett. **91**, 152505 (2007).
[15]S. Mangin, D. Ravelosona, J. A. Katine, M. J. Carey, B. D. Terris, and E. E. Fullerton, Nature Mater. **5**, 210 (2006).
[16]S. Park, N. M. Nguyen, C. Burrowes, E. E. Fullerton, C. Chappert, L. Prejebeanu, F. Garcia-Sanchez, and D. Ravelosona, Appl. Phys. Lett. **98**, 232512 (2011).
[17]A. Baruth, L. Yuan, J. D. Burton, K. Janicka, E. Y. Tsymbal, S. H. Liou, and S. Adenwalla, Appl. Phys. Lett. **89**, 202505 (2006).
[18]S. Wiebel, J. P. Jamet, N. Vernier, A. Mougin, J. Ferre, V. Baltz, B. Rodmacq, and B. Dieny, Appl. Phys. Lett. **86**, 142502 (2005).
[19]T. Hauet, C. M. Gunther, B. Pfau, M. E. Schabes, J. U. Thiele, R. L. Rick, P. Fischer, S. Eisebitt, and O. Hellwig, Phys. Rev. B **77**, 184421 (2008).
[20]Z. Y. Liu, F. Zhang, N. Li, B. Xu, D. L. Yu, J. L. He, and Y. J. Tian, J. Appl. Phys. **104**, 113903 (2008).
[21]K. M. Döbrich, M. Wietstruk, J. E. Prieto, F. Heigl, O. Krupin, K. Starke, and G. Kaindl, Phys. Rev. Lett. **100**, 227203 (2008).
[22]P. Poulopoulos, U. Bovensiepen, M. Farle, and K. Baberschke, Phys. Rev. B **57**, R14036 (1998).
[23]P. J. Metaxas, P. J. Zermatten, J. P. Jamet, J. Ferre, G. Gaudin, B. Rodmacq, A. Schuhl, and R. L. Stamps, Appl. Phys. Lett. **94**, 132504 (2009).
[24]A. O. Adeyeye and N. Singh, J. Phys. D: Appl. Phys. **41**, 153001 (2008).
[25]I. Kato, S. Takei, X. X. Liu, and A. Morisako, IEEE. Trans. Magn. **42**, 2366 (2006).
[26]J. M. Shaw, H. T. Nembach, T. J. Silva, S. E. Russek, R. Geiss, C. Jones, N. Clark, T. Leo, and D. J. Smith, Phys. Rev. B **80**, 184419 (2009).
[27]J. Kanak, M. Czapkiewicz, T. Stobieckf, M. Kachel, I. Sveklo, A. Maziewski, and S. van Dijken, Phys. Status Solidi **204**, 3950 (2007).
[28]S. K. Wong, B. H. Chia, K. Srinivasan, R. Law, E. L. Tan, H. K. Tan, R. Sbiaa, and S. N. Piramanayagam, J. Appl. Phys. **106**, 093904 (2009).
[29]G. Herzer, IEEE. Trans. Magn. **26**, 1397 (1990).
[30]T. Thomson, G. Hu, and B. D. Terris, Phys. Rev. Lett. **96**, 257204 (2006).
[31]J. M. Shaw, M. Olsen, J. W. Lau, M. L. Schneider, T. J. Silva, O. Hellwig, E. Dobisz, and B. D. Terris, Phys. Rev. B **82**, 144437 (2010).
[32]C.-H. Lai, C. J. Chen, and T. S. Chin, J. Appl. Phys. **89**, 6928 (2001).
[33]H. Yuasa, M. Hara, and H. Fukuzawa, Appl. Phys. Lett. **92**, 262509 (2008).
[34]J. Norpoth *et al*., J. Phys. D: Appl. Phys. **41**, 025001 (2008).
[35]R. Engel-Herbert and T. Hesjedal, J. Appl. Phys. **97**, 074504 (2005).
[36]A. P. Mihai, J. P. Attane, A. Marty, P. Warin, and Y. Samson, Phys. Rev. B **77**, 060401 (2008).
[37]H. Nemoto, H. Nakagawa, and Y. Hosoe, IEEE. Trans. Magn. **39**, 2714 (2003).
[38]J. W. Knepper and F. Y. Yang, Phys. Rev. B **71**, 224403 (2005).
[39]S. M. Mohseni, R. K. Dumas, Y. Fang, J. W. Lau, S. R. Sani, J. Persson, and J. Akerman, Phys. Rev. B. **84**, 174432 (2011).
[40]G. Feng, H. C. Wu, J. F. Feng, and J. M. D. Coey, Appl. Phys. Lett. **99**, 042502 (2011).
[41]F. Zhang, F. S. Wen, L. Li, N. Wang, Y. F. Lu, Z. Y. Liu, B. Xu, D. L. Yu, J. L. He, and Y. J. Tian, Thin Solid Films **519**, 1980 (2011).
[42]M. V. Costache, G. Bridoux, I. Neumann, and S. O. Valenzuela, Nature Mater. **11**, 199 (2012).